Electronic Supplementary Material (ESI) for Nanoscale.

# Supplementary Information for

# Modulating electrocatalytic $CO_2$ reduction performances of bismuth nanoparticles with carbon substrates of controlled oxidation degrees

Si-Qian Wu[1], Yu-Chen Hao[1], Li-Wei Chen[1], Jiani Li[1], Zi-Long Yu[1], Zhejiaji Zhu[1], Di Liu[1], Xin Su[1], Linyu Hu[1], Hui-Zi Huang[1] and An-Xiang Yin*[1]

[1]Ministry of Education Key Laboratory of Cluster Science, Beijing Key Laboratory of Photoelectronic/Electrophotonic Conversion Materials, Advanced Technology Research Institute (Jinan), School of Chemistry and Chemical Engineering, Beijing Institute of Technology, Beijing 100081, P. R. China

## Experimental section

### Chemicals and materials

Bismuth nitrate pentahydrate ($Bi(NO_3)_3·5H_2O$, 98%), sodium borohydride ($NaBH_4$, 96%), ethylene glycol ($C_2H_6O_2$, 99%), carbon black (CB, acetylene black, 99.9%), and potassium bicarbonate ($KHCO_3$, 99.5%) were purchased from Alfa Aesar (USA). Sulfuric acid ($H_2SO_4$, 98%), hydrogen peroxide ($H_2O_2$, 30%), hydrochloric acid (HCl, 36%~37%), and ethanol ($C_2H_6O$, 99%) were purchased from Beijing Chemical Reagent Co. Ltd. (China). Potassium permanganate ($KMnO_4$, >99%) was purchased from Sigma Aldrich (USA). Nafion solution (5% in methanol) was purchased from DuPont (USA). Potassium hydroxide (KOH, 95%), Deuterated water ($D_2O$, 99.9%) and dimethyl sulfoxide (DMSO, 99.8%) were purchased from Aladdin Co. Ltd. (China). All regents were used directly without any further purification. The carbon paper (CP, TGP-H-090) was purchased from TORAY (Japan). The deionized water with a specific resistance of 18.2 MΩ·cm was obtained by a Milli-Q system. Argon (Ar, 99.999%) was purchased from APBAIF Gases Industry Co. Ltd. (China) and $CO_2$ (99.999%) was purchased from Beiwen Gases Co. Ltd. (China).

The CP (TORAY) was washed by ethanol and ultrapure water several times and then dried at 40 °C before use. The Nafion 115 membrane (DuPont) was pretreated in 5% $H_2O_2$ solution (80 °C) for 1 h, in 0.05 M $H_2SO_4$ solution for 3 h, then in ultrapure water (80 °C) for another 1 h, and finally washed with ultrapure water several times before use.

### Methods

### Preparation of mildly oxidized CB

CB were mildly oxidized by a modified Hummers' method.[1] Typically, 1 g of CB was annealed at 500 °C in air for 2 h and washed with 40 mL of diluted hydrochloric acid (10 wt.%) to remove the metal residues and amorphous carbon. The purified CB were repeatedly washed with water and then collected. After drying overnight, ∼23 mL of concentrated sulfuric acid was mixed with the purified CB (~1 g) in a 250 mL round flask and stirred at room temperature for 12 h. Subsequently, the round flask was heated to 40 °C in an oil bath, followed by the slow addition of ∼1 g of $KMnO_4$ with continuous stirring. After stirring at 40 °C for 30 min, 3 mL of water was added, followed by another 3 mL after 5 min. A 40 mL portion of water was slowly added 5 min later to keep the temperature below 45 °C. After 15 min, 140 mL of water was poured into the solution at room temperature, followed by the addition of 10 mL of 30% $H_2O_2$ to stop the reaction after 10 min. The mildly oxidized CB (denoted as $CB_1$ in the main text and SI) were collected, washed with diluted HCl solution (5 wt.%) twice, and then with water repeatedly until the pH value of the rinsing solution is equal to or higher than 5. The final suspension (in $H_2O$) was lyophilized to obtain solid powders of $CB_1$.

The preparation of oxidized $CB_3$ and $CB_5$ followed similar procedures except that the mass of $KMnO_4$ was increased to 3 and 5 g, respectively.

### Preparations of Bi/CB catalysts

Typically, 10 mg of $CB_1$ was fully dispersed in 10 mL of anhydrous ethylene glycol and sonicated for 30 min before the addition of 5 mL of ethylene glycol solution of 1.0 mM $Bi(NO_3)_3\cdot 5H_2O$. The mixture solution was vigorously stirred for 12 h, sonicated for another 30 min, and then transferred to a 25 mL Teflon-lined stainless-steel autoclave. After a solvothermal reaction at 180 °C for 16 h, the final product ($Bi/CB_1$) was collected by centrifugation (8000 rpm, 5 min), washed with 0.1 M $NaBH_4$ ethanol solution twice and with ethanol several times, and then dried under vacuum at room temperature.

The synthesis of $Bi/CB_0$, $Bi/CB_3$, and $Bi/CB_5$ followed similar procedures except that $CB_1$ was replaced with untreated CB (denoted as $CB_0$), $CB_3$, and $CB_5$, respectively.

### Characterizations

Powder X-ray diffraction (PXRD) patterns were collected on a Rigaku MiniFlex 600 diffractometer with a Cu Kα X-ray radiation source (λ= 0.154056 nm) at the scan rate of 5 ° $min^{-1}$. Fourier transform infrared (FT-IR) spectra were collected on a Perkin Elmer Frontier spectrometer (resolution: 4 $cm^{-1}$). $^1H$ nuclear magnetic resonance (NMR) spectra were recorded on a Bruker Ascend 400 (400 MHz) spectrometer. Deuterium oxide was used for deuterated reagent. Inductively coupled plasma-atomic emission spectroscopy (ICP-AES) studies were performed on an Agilent ICP-AES 720 spectrometer. X-ray photoelectron spectroscopy (XPS) studies were carried out on a Thermo Fisher Scientific ESCALAB 250 Xi photoelectron spectrometer with a monochromatic Al Kα radiation (hν = 1486.6 eV), using the binding energy of C 1*s* peak at 284.8 eV as reference. The as-synthesized sample was placed in a chamber filled with argon to protect the bismuth particles from oxidation by the air. Transmission electron microscopy (TEM) and high-resolution (HRTEM) studies were performed on a JEOL JEM-2100 transmission electron microscope operating at 200 kV.

### Electrochemical measurements

All the electrochemical measurements were conducted on the CHI 660E electrochemical station (Chenhua, Shanghai) in a typical two-compartment electrolysis cell with the three-electrode configuration. The cathodic and anodic compartments were separated by the proton exchange membrane (Nafion 115), each containing 35 mL of electrolytes (0.5 M $KHCO_3$).

Typically, the catalyst ink was prepared by dispersing 3 mg of Bi/CB (i.e., $Bi/CB_0$, $Bi/CB_1$, $Bi/CB_3$, and $Bi/CB_5$) powders and 30 μL of Nafion solution in the mixture of water (75 μL) and isopropanol (25 μL) under sonication (20 min). Then, about 30 μL of the catalyst inks were applied onto the pretreated CP (0.6 cm × 1.2 cm) in a dropwise manner and dried at room temperature to serve as the working electrode, with a Bi/CB mass loading of about 1 mg $cm^{-2}$. A platinum plate (1 cm ×1 cm) and a saturated calomel electrode (SCE) electrode were used the counter electrode and the reference electrode, respectively. All the electrochemical measurements were conducted under normal pressure and room temperature, and the electrode potentials were converted to versus the reversible hydrogen electrode (RHE) scale through the following equation.

$$\mathrm{E\ (V\ versus\ RHE) = E\ (V\ versus\ SCE) + 0.0591 \times pH + 0.241} \tag{1}$$

Linear sweep voltammetry (LSV) measurements (scan rate: 10 mV $s^{-1}$) were carried out in Ar or $CO_2$-saturated electrolytes by bubbling Ar or $CO_2$ into the cathodic electrolytes for 30 min before the measurements, respectively. Before LSV measurements, cyclic voltammetry (CV) tests ( −1.1 V~ −0.1 V, 50 mV $s^{-1}$, 20 cycles) were carried out to activate the working electrode.

For $CO_2$ electrolysis tests, high purity (99.999%) $CO_2$ gas was bubbled in to the cathodic electrolytes at the rate of 50 mL $min^{-1}$. The electrolytes were magnetically stirred at the rate of 800 rpm during the measurements. Electrochemical impedance spectroscopy (EIS) was performed from 0.01 Hz to 1,000,000 Hz at −0.9 V vs. RHE in $CO_2$-saturated 0.5 M $KHCO_3$ electrolytes. The Tafel slopes for formate generation on Bi/CB catalysts were derived from the effective current densities for formate formation at different cathodic potentials.[2-3]

Gaseous products were quantified by an online gas chromatograph (GC, SHIMADZU 2014C) with a thermal conductivity detector (TCD) and a flame ionization detector (FID). $^1H$ nuclear magnetic resonance (NMR) spectroscopy was employed to quantify the liquid products after the electrolysis. In general, 500 μL of electrolytes were extracted from the cathodic cell after electrocatalysis and mixed with 100 μL $D_2O$. Then, 100 μL DMSO solution (500 ppm) was added as the internal standard. The one-dimensional $^1H$ spectrum was measured using a solvent pre-saturation method to suppress the water peak.[4]

## Calculation methods

The Faradaic efficiency (FE) values for CO and $H_2$ were calculated from the equation:

$$\mathrm{FE} = \frac{2n_g \times F}{i} = \frac{2pfx_gF/RT}{i} \tag{2}$$

where $n_g$ is the formation rate of gas g (mol $s^{-1}$), $f$ is the gas flow rate ($m^3$ $s^{-1}$), $x_g$ is the faction of gas g detected by GC, $F$ is the Faraday constant (96485 C $mol^{-1}$), $R$ is the gas constant (8.314 J $mol^{-1}K^{-1}$), $i$ is the stable current of the chronoamperometry test, $p$ is 101.325 kPa, and T is 295.15 K.

The FE of formate was calculated from the equation:

$$FE_{formate} = V \times c \times \frac{nF}{Q} \qquad (3)$$

where $V$ is the volume of the electrolyte in the cathode cell (cm$^3$), $c$ is the concentration of formate after electrolysis, determined by $^1$H NMR (mol mL$^{-1}$), $n = 2$ is the number of transferred electrons for formate, $F$ is the Faraday constant (96485 C mol$^{-1}$), and $Q$ is the total charge passed through the cathode in the electrolysis (C).

The partial current density of formate ($j_{\text{formate}}$) was calculated as follows:

$$j_{\text{formate}} = j_{\text{total}} \times \text{FE}_{\text{formate}} \qquad (4)$$

where $j_{\text{total}}$ is the total current density obtained from the chronoamperometry tests.

## Additional Figures and Tables

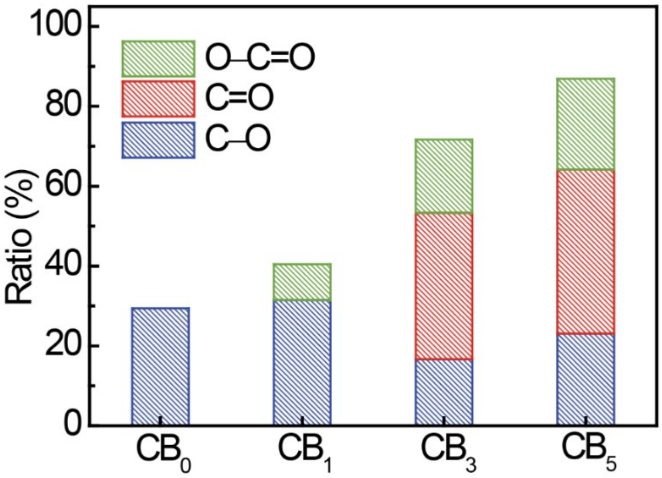

**Figure S1.** The ratio of C–O, C=O, O–C=O area to C–C area in $CB_0$, $CB_1$, $CB_3$ and $CB_5$ respectively calculated from the deconvoluted XPS C 1s. (divide the integrated peak area of C−O, C=O and O−C=O by the integrated peak area of C–C).

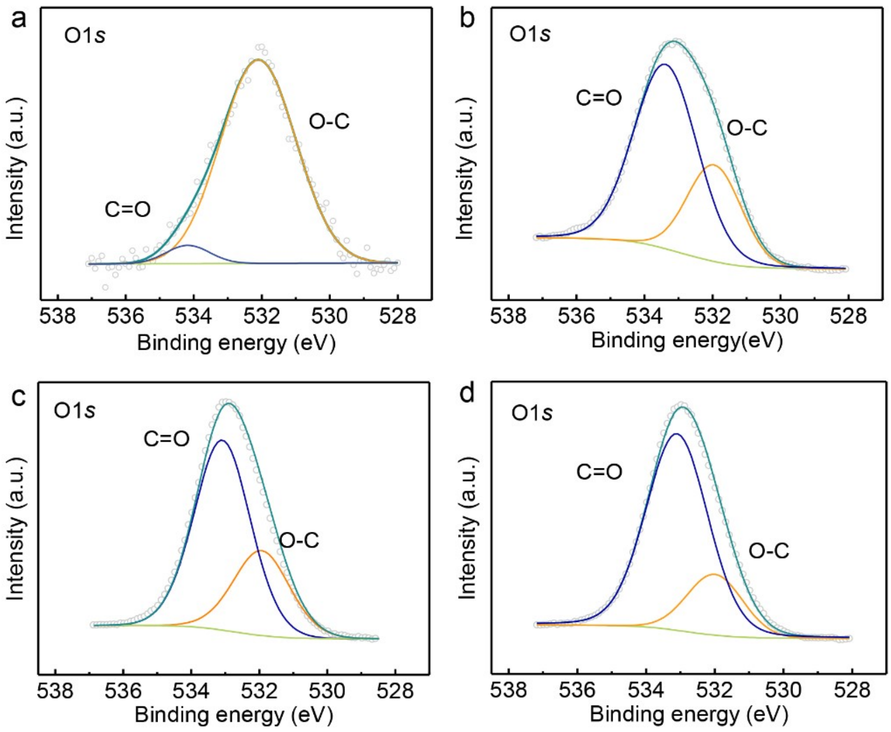

**Figure S2.** O 1*s* core level XPS spectra for (a) $CB_0$, (b) $CB_1$, (c) $CB_3$, and (d) $CB_5$.

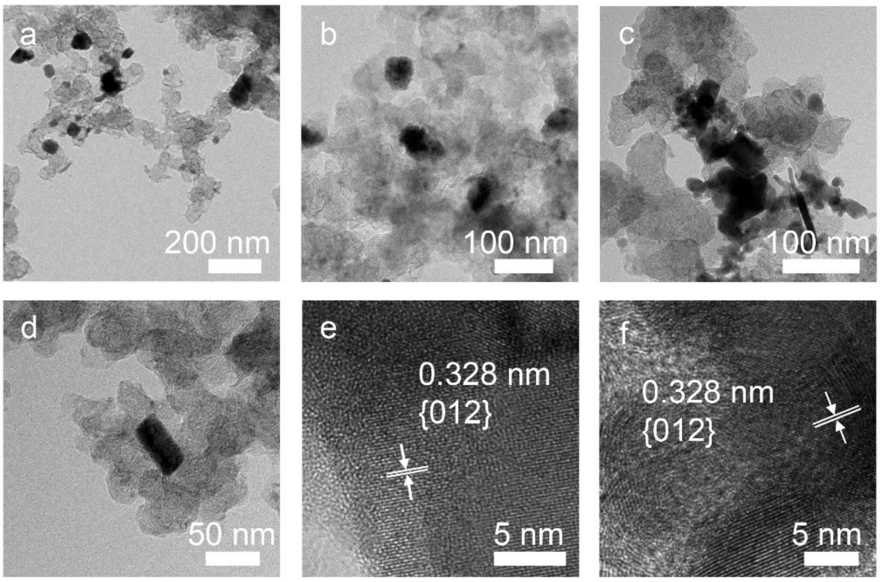

**Figure S3.** Morphology and structure characterizations of Bi/CB$_0$. TEM images (a–d) and HRTEM images (e–f) of Bi/CB$_0$ sample.

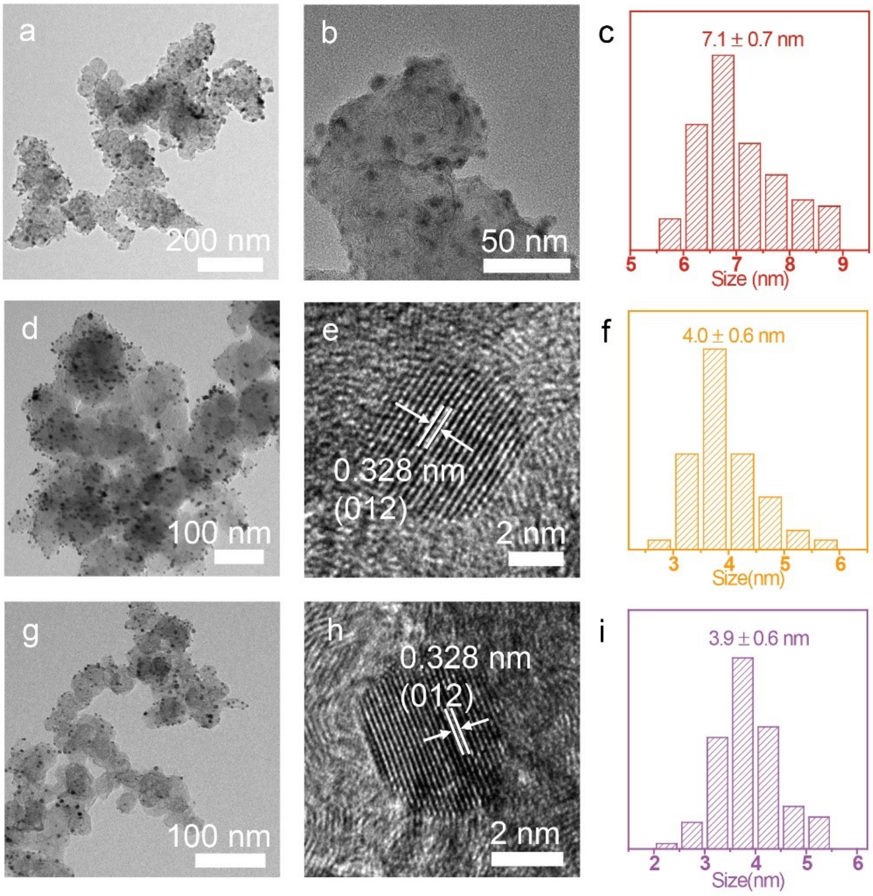

**Figure S4.** Morphology and structure characterizations of different Bi/CB samples. (a, b) TEM images of Bi/CB$_1$, (d, e) TEM and HRTEM images for Bi/CB$_3$, and (g, h) TEM and HRTEM images for Bi/CB$_5$. (c, f, i) Size distributions for Bi/CB$_1$, Bi/CB$_3$ and Bi/CB$_5$ (collected from more than 100 Bi nanoparticles).

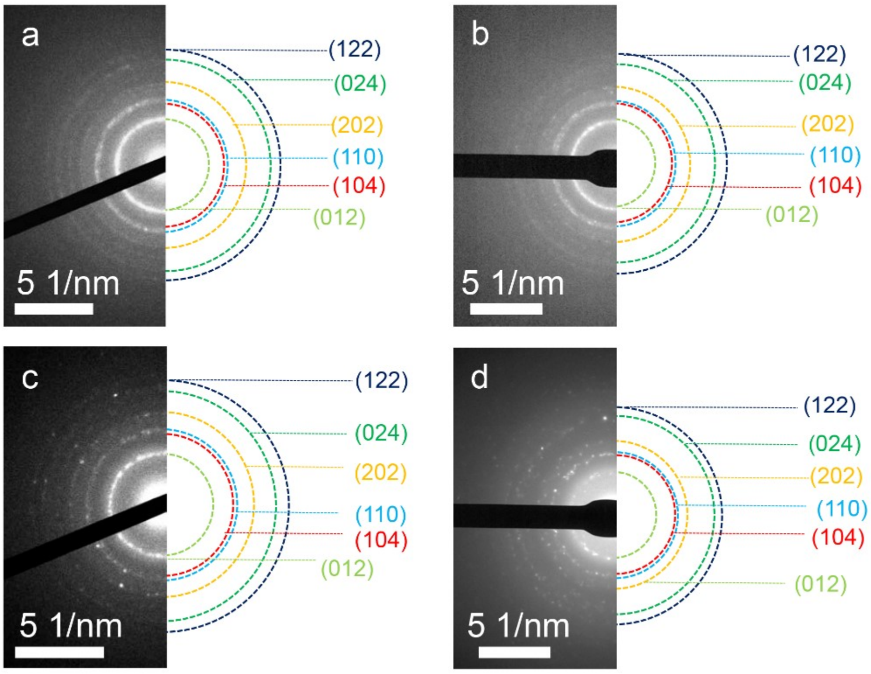

**Figure S5.** Selected area electron diffraction (SAED) pattern of BiNPs/CB. (a) Bi/CB$_0$, (b) Bi/CB$_1$, (c) Bi/CB$_0$ and (d) Bi/CB$_5$.

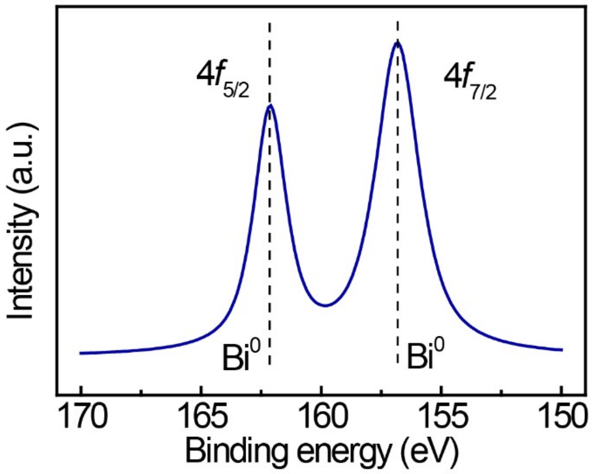

**Figure S6.** XPS profiles for the as-obtained Bi/CB$_1$, suggesting that the obtained BiNPs were mainly in the metallic state.

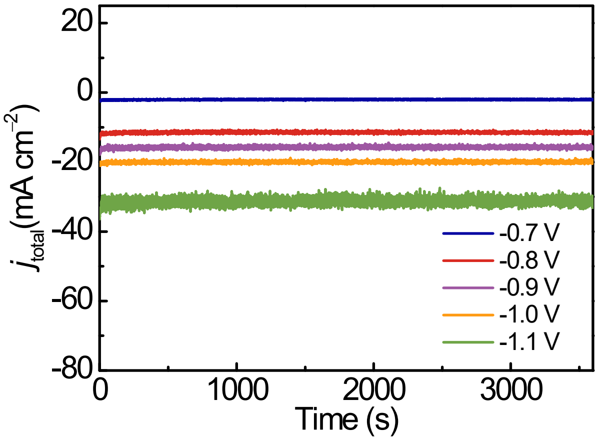

**Figure S7.** Chrono-amperometry results at various cathodic potentials for Bi/CB$_1$ in CO$_2$-saturated 0.5 M KHCO$_3$ solutions.

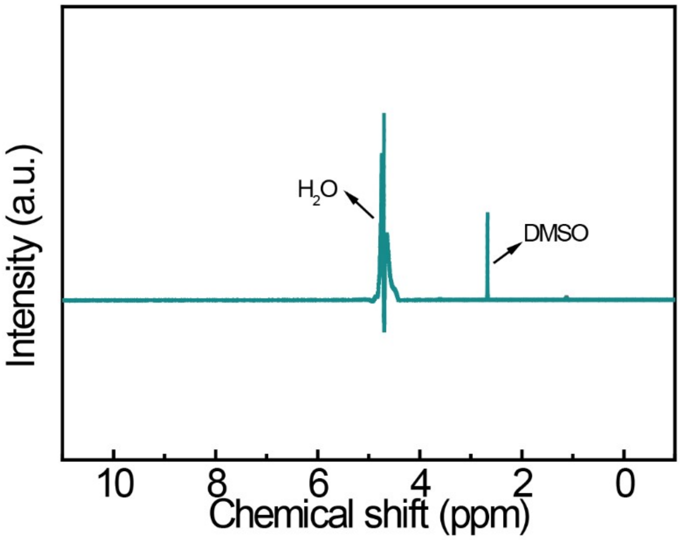

**Figure S8.** Representative NMR spectrum for the electrolyte extracted from the cathodic compartment after 1 h of electrolysis reactions on Bi/$CB_1$ at −0.9 V vs. RHE in Ar-saturated 0.5 M $KHCO_3$ solution. No formate species could be detected by NMR.

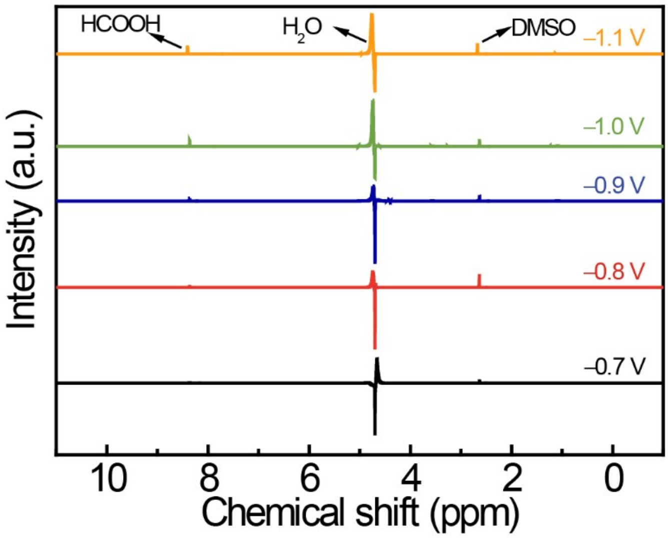

**Figure S9.** Representative NMR spectra for the electrolytes extracted from the cathodic compartment after 1 h of electrolysis reactions on $Bi/CB_1$ at −0.7 V, −0.8 V, −0.9 V, −1.0 V and −1.1 V vs. RHE in $CO_2$-saturated 0.5 M $KHCO_3$ solution. Formate species could be detected when the cathodic potential was lower than or equal to −0.7 V vs. RHE.

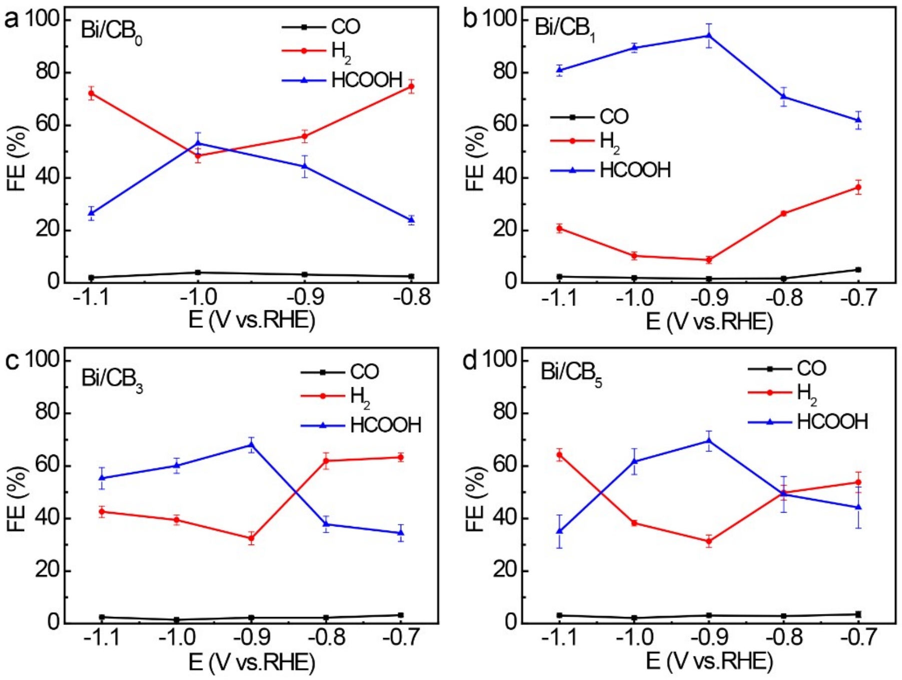

**Figure S10.** Potential-dependent Faradaic efficiency values for carbon oxide, hydrogen, and formate on Bi/CB$_0$, Bi/CB$_1$, Bi/CB$_3$ and Bi/CB$_5$, respectively. The error bars indicate the standard deviations of at least three independent experiments.

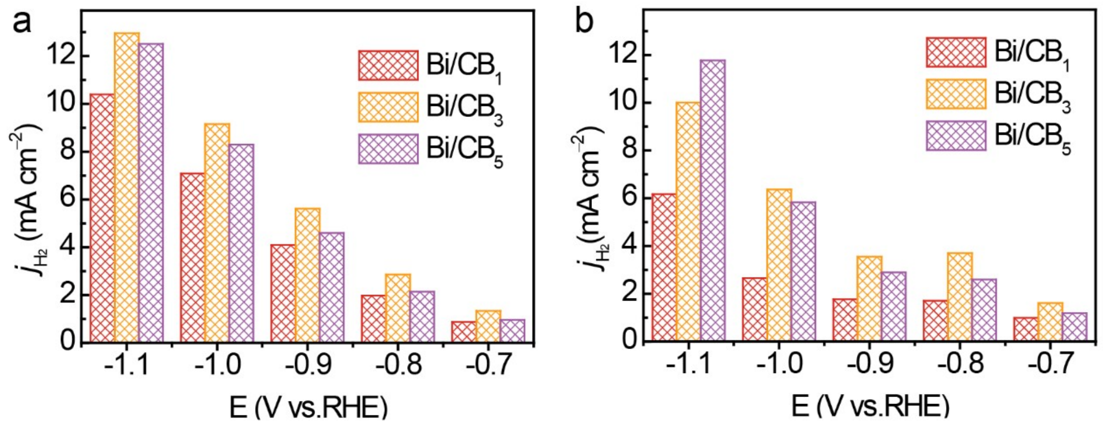

**Figure S11.** Partial current densities for $H_2$ production ($j_{H_2}$) over Bi/CB$_1$, Bi/CB$_3$, and Bi/CB$_5$ in **(a)** Ar-saturated and **(b)** $CO_2$-saturated 0.5 M $KHCO_3$ solutions. Hydrogen evolution was effectively suppressed on Bi/CB$_1$, as compared with other two samples.

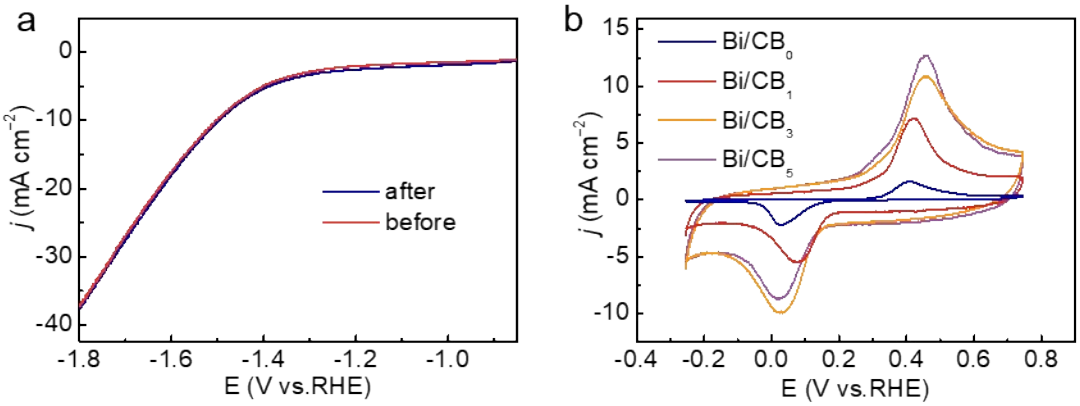

**Figure S12.** (a) LSV curves for Bi/CB$_1$ before and after 1 h of electrocatalytic $CO_2$RR reaction. (b) CV curves (scan rate: 20 mV s$^{-1}$) for Bi/CB$_0$, Bi/CB$_1$, Bi/CB$_3$ and Bi/CB$_5$ in Ar-saturated 0.5 M $KHCO_3$ solution, respectively.

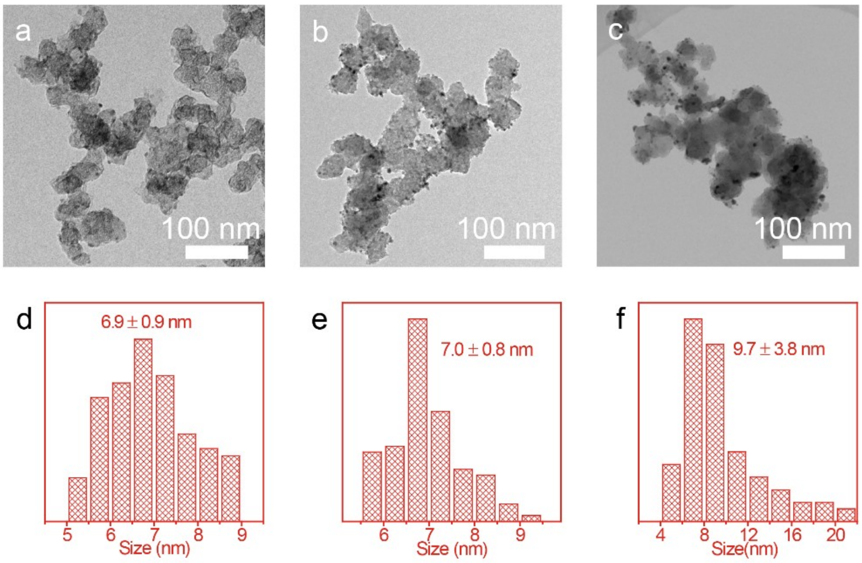

**Figure S13.** TEM images and size distributions (collected from more than 100 Bi nanoparticles) of Bi/CB$_1$ after (a) 6 h, (b) 16 h, and (c) 24 h of CO$_2$RR with the cathodic potential of −0.9 V vs. RHE.

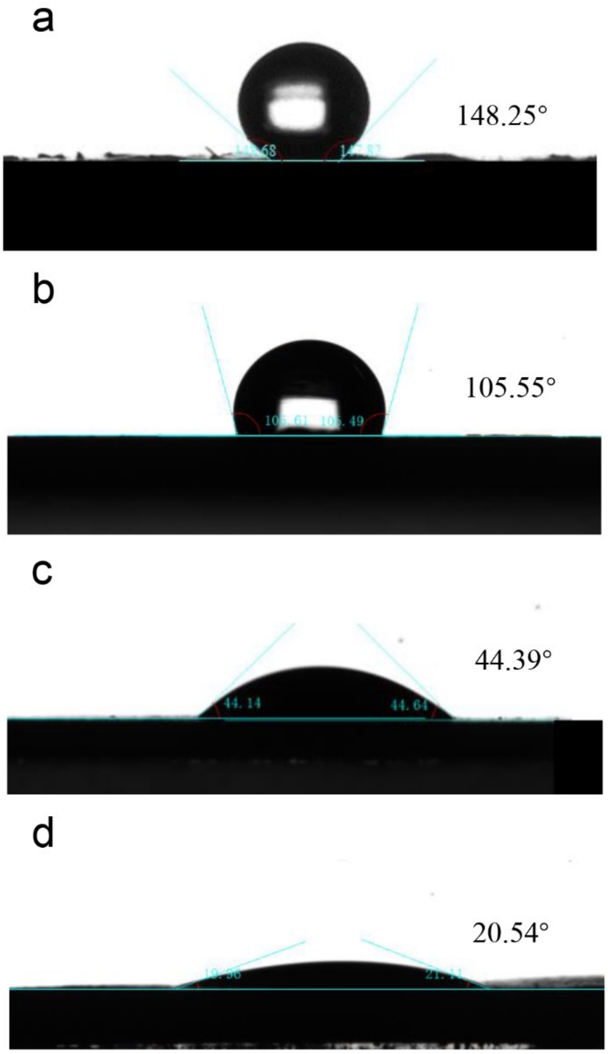

**Figure S14.** Photographs of water droplet contact angles on four different samples (Bi/CB$_0$, Bi/CB$_1$, Bi/CB$_3$ and Bi/CB$_5$).

**Table S1.** The nominal and actual loadings of Bi and average particle size in different Bi/C catalysts.

| **Catalysts** | **Bi loading (wt%)** | | **Bi particle size (nm)** |
|---|---|---|---|
| | **nominal** | **ICP-AES** | **TEM** |
| Bi/CB-1 | 10 | 6.18 | 7.1 ± 0.7 |
| Bi/CB-3 | 10 | 6.32 | 4.0 ± 0.6 |
| Bi/CB-5 | 10 | 6.30 | 3.9 ± 0.6 |

**Table S2.** The estimated surface area ($S_A$, m $^2$ g$^{-1}$) for different catalysts (Bi/CB$_1$, Bi/CB$_3$ and Bi/CB$_5$).

|  | **Size distribution (×10$^{-9}$ m)** | **Density (×10$^6$ g m$^{-3}$ )** | **Atomic radius (×10$^{-12}$ m)** | **$S_A$ (m$^2$ g$^{-1}$ )** |
|---|---|---|---|---|
| Bi/CB-1 | 7.1 ± 0.7 | 9.8 | 160 | 86.2 |
| Bi/CB-3 | 4.0 ± 0.6 |  |  | 153.0 |
| Bi/CB-5 | 3.9 ± 0.6 |  |  | 157.0 |

**Table S3.** Electrocatalytic performances for $CO_2$ to formate in H-type cell over the state-of-the-art Bi-based electrocatalysts.

| **Electrocatalysts** | **Electrolyte** | **Potential** | **$FE_{formate}$** | **$j_{formate}$** | **Ref.** |
|---|---|---|---|---|---|
| **$Bi/CB_1$** | **0.5 M $KHCO_3$** | **–0.9 V vs. RHE** | **94%** | **16.7 mA $cm^{-2}$** | **This work** |
| Electrodeposited Bi dendrites | 0.5 M $NaHCO_3$ | –1.8 V vs. SCE | 96.4% | 14.6 mA $cm^{-2}$ | 5 |
| Hierarchical Bi dendrites | 0.5 M $KHCO_3$ | –0.74 V vs. RHE | 89% | 2.4 mA $cm^{-2}$ | 6 |
| $BiO_x/C$ | 0.5 M $KHCO_3$ | –1.7 V vs. Ag/AgCl | 93.4% | 14.8 mA $cm^{-2}$ | 7 |
| Mp-Bi | 0.5 M $NaHCO_3$ | –0.9 V vs. RHE | 100% | 15 mA $cm^{-2}$ | 8 |
| Bi nanoparticles | 0.5 M $KHCO_3$ | –0.83 V vs. RHE | 94.7% | 4.9 mA $cm^{-2}$ | 9 |
| Ultrathin Bi nanosheets | 0.5 M $NaHCO_3$ | –1.6 V vs. SCE | 95% | 15–16 mA $cm^{-2}$ | 10 |
| Bi nanosheets | 0.1 M $KHCO_3$ | –1.1 V vs. RHE | 86% | 16.5 mA $cm^{-2}$ | 11 |
| $Bi_2O_2CO_3$ | 0.5 M $NaHCO_3$ | –0.9 V vs. RHE | 95% | 11 mA $cm^{-2}$ | 12 |
| Sulfide-derived Bi | 0.5 M $NaHCO_3$ | –0.75 V vs. RHE | 84% | 4.2 mA $cm^{-2}$ | 13 |
| BiOBr-derived Bi | 0.1 M $KHCO_3$ | –0.9 V vs. RHE | 95% | 60 mA $cm^{-2}$ | 14 |
| $Bi_2O_3$NSs@MCCM | 0.1 M $KHCO_3$ | –1.256 V vs. RHE | 93.8% | 15 mA $cm^{-2}$ | 15 |
| AgBi-500 | 0.1 M $KHCO_3$ | –0.7 V vs. RHE | 94.3% | 12.52 mA $cm^{-2}$ | 16 |
| BiNP@MWCNT | 0.5 M KHCO3 | –1.5 V vs. SCE | 95.2% | 10.7 mA $cm^{-2}$ | 17 |
| $Bi_2O_3$@C | 0.5 M $KHCO_3$ | –0.9 V vs. RHE | 92% | 7.5 mA $cm^{-2}$ | 18 |
| $Bi_2S_3$-$Bi_2O_3$@rGO | 0.5 M $KHCO_3$ | –0.9 V vs. RHE | 90% | 3.5 mA $cm^{-2}$ | 19 |
| Bismuthene | 0.5 M $KHCO_3$ | –0.58 V vs. RHE | 98% | 2.9 mA $cm^{-2}$ | 20 |
| BiSA/C | 0.1 M $KHCO_3$ | –1.1 V vs. RHE | 83.6% | NA | 21 |
| Bi/rGO | 0.1 M $KHCO_3$ | –0.8 V vs. RHE | 98% | 1.8 mA $cm^{-2}$ | 22 |
| $S_2$-$Bi_2O_3$-CNT | 0.5 M $KHCO_3$ | –0.9 V vs. RHE | 90% | 28 mA $cm^{-2}$ | 23 |

## References

1. D. Y.Wang, M. Gong, H. L. Chou, C. J. Pan,; H. A. Chen and H. Dai, *J. Am. Chem. Soc.* 2015, **137** (4), 1587–1592.
2. K. Fan, Y. Jia, Y. Ji, P. Kuang, B. Zhu, X. Liu and J. Yu, *ACS Catal.* 2019, **10** (1), 358–364.
3. Y. X. Duan, Y. T. Zhou, Z. Yu, D. X. Liu, Z. Wen, J. M. Yan and Q. Jiang, *Angew. Chem. Int. Ed.* 2021, **60** (16), 8798–8802.
4. W. S. Price, *Annual Reports on NMR Spectroscopy* 1999, **38**, 289–354.
5. H. Zhong, Y. Qiu, T. Zhang, X. Li, H. Zhang and X. Chen, *J. Mater. Chem. A* 2016, **4** (36), 13746–13753.
6. J. H. Koh, D. H.Won, T. Eom, N. Kim, K. Jung, H. Kim, Y. J. Hwang and B. K. Min, *ACS Catal.* 2017, **7**, 5071–5077.
7. C. W. Lee, J. S. Hong, K. D. Yang, K. Jin, J. H. Lee, H.-Y. Ahn, H. Seo, N.-E. Sung and K. T. Nam, *ACS Catal.* 2018, **8** (2), 931–937.
8. H. Yang, N. Han, J. Deng, J. Wu, Y. Wang, Y. Hu, P. Ding, Y. Li, Y. Li and J. Lu, *Adv. Energy Mater.* 2018, **8**, 1801536.
9. X. Zhang, X. Hou, Q. Zhang, Y. Cai, Y. Liu and J. Qiao, *J. Catal.* 2018, **365**, 63–70.
10. N. Han, Y. Wang, H. Yang, J. Deng, J. Wu, Y. Li and Y. Li, *Nat. Commun.* 2018, **9**, 1320.
11. W. Zhang, Y. Hu, L. Ma, G. Zhu, P. Zhao, X. Xue, R. Chen, S. Yang, J. Ma, J. Liu and Z. Jin, *Nano Energy* 2018, **53**, 808–816.
12. Y. Zhang, X. L. Zhang, Y. Z. Ling, F. W. Li, Alan M. Bond and J. Zhang, *Angew. Chem. Int. Ed.* 2018, **57**, 13283–13287.
13. Y. Zhang, F. Li, X. Zhang, T. Williams, C. D. Easton, A. M. Bond and J. Zhang, *J. Mater. Chem. A* 2018, **6** (11), 4714–4720.
14. F. P. Garcia de Arquer, O. S. Bushuyev, P. De Luna, C. T. Dinh, A. Seifitokaldani, M. I. Saidaminov, C. S. Tan, L. N. Quan, A. Proppe, M. G. Kibria, S. O. Kelley, D. Sinton and E. H. Sargent, *Adv. Mater.* 2018, **30** (38), e1802858.
15. S. Liu, X. F. Lu, J. Xiao, X. Wang and X. W. Lou, *Angew. Chem. Int. Ed.* 2019, **58** (39), 13828–13833.
16. J. H. Zhou, K. Yuan, L. Zhou, Y. Guo, M. Y. Luo, X. Y. Guo, Q. Y. Meng and Y. W. Zhang, *Angew. Chem. Int. Ed.* 2019, **58** (40), 14197–14201.
17. X. Zhang, J. Fu, Y. Liu, X. D. Zhou and J. Qiao, *ACS Sustain Chem Eng.* 2020, **8** (12), 4871–4876.
18. P. Deng, F. Yang, Z. Wang, S. Chen, Y. Zhou, S. Zaman and B. Y. Xia,, *Angew. Chem. Int. Ed.* 2020, **59** (27), 10807–10813.
19. X. Yang, P. Deng, D. Liu, S. Zhao, D. Li, H. Wu, Y. Ma, B. Y. Xia, M. Li, C. Xiao and S. Ding, *J. Mater. Chem. A* 2020, **8** (5), 2472–2480.

20. F. Yang, A. O. Elnabawy, R. Schimmenti, P. Song, J. Wang, Z. Peng, S. Yao, R. Deng, S. Song, Y. Lin, M. Mavrikakis and W. Xu, *Nat. Commun.* 2020, **11**, 1088.

21. X. Yang, Y. Chen, L. Qin, X. Wu, Y. Wu, T. Yan, Z. Geng and J. Zeng, *ChemSusChem* 2020, **13** (23), 6307–6311.

22. Y. X. Duan, K. H. Liu, Q. Zhang, J. M. Yan and Q. Jiang, *Small Methods* 2020, **4**, 1900846.

23. S. Q. Liu,; M. R. Gao, R. F. Feng, L. Gong, H. Zeng, J. L. Luo, *ACS Catal.* 2021, **11** (12), 7604–7612.